INTERNATIONAL ATOMIC ENERGY AGENCY
UNITED NATIONS EDUCATIONAL, SCIENTIFIC AND CULTURAL ORGANIZATION

INTERNATIONAL CENTRE FOR THEORETICAL PHYSICS
34100 TRIESTE (ITALY) - P.O. BOX 586 - MIRAMARE - STRADA COSTIERA 11 - TELEPHONES: 224281/2/3/4/5/6
CABLE: CENTRATOM - TELEX 460892-1

SMR/164-4

AUTUMN WORKSHOP

IN

CLOUD PHYSICS AND CLIMATE

25 November - 20 December 1985

THE GENERAL ATMOSPHERIC CIRCULATION AND CLIMATES OF ARID ZONES

R.P. PEARCE

Department of Meteorology
University of Reading
2 Earley Gate
Whiteknights
P.O. Box 239
Reading, RG6 2AU
Berks
U.K.

THE GENERAL ATMOSPHERIC CIRCULATION AND CLIMATES OF ARID ZONES

R.P. Pearce
Department of Meteorology
University of Reading

LECTURE 1 CLIMATE VARIABLES AND THEIR CALCULATION; THE ATMOSPHERIC HEAT BALANCE

1.1 Climate variables

An understanding of the atmospheric general circulation is essential to an understanding of climate. One of the first comprehensive climatologies of the atmosphere, treating it as a fully three-dimensional physical system, was that published in 1972 and 1974 by Newell, Kidson, Vincent and Boer (NKVB). Their emphasis was on the tropics and, despite the poor coverage of observations, they were able to make useful estimates of such dynamically significant quantities as vertical motion and eddy transfers of heat, moisture and momentum. The main component of their data base consisted of daily station values of wind components (u,v), temperature (T), isobaric height (z) and specific humidity (q) over the globe for the years 1957-64, supplied by the U.S. National Weather Records Centre. The basic data were then first combined into time-average values, viz: $\bar{u}$, $\bar{v}$, $\bar{T}$, $\bar{z}$, $\bar{q}$, $\overline{u'v'}$, $\overline{u'T'}$, $\overline{v'T'}$, $\overline{u'z'}$, $\overline{v'z'}$, $\overline{u'q'}$, $\overline{v'q'}$, where the bar denotes a time average and the prime a deviation (standard deviations $\sigma(u)$, $\sigma(v)$, $\sigma(T)$ and $\sigma(q)$ were also calculated) and zonal averages, e.g. $[u]$, $[T]$, $[u'v']$ with standing eddy components $\bar{u}^*$, $\bar{T}^*$, etc.

Fields of $\bar{T}$ at 1000 mb for the tropical strip for Dec-Feb and Jun-Aug obtained by NKVB are shown in Fig. 1. Note the substantial warming over the N. Hemisphere land surfaces and over Australia in summer. Fields of $[\bar{u}]$ for Dec-Feb and Jun-Aug are shown in Fig. 2; the main features are the well-known subtropical jets and surface belts of tropical easterlies and mid-latitude westerlies.

The zonal mean vertical motion is inferred from the $\bar{v}(\phi,p)$ distribution (p the pressure and ϕ the latitude) using the zonally- and time-averaged form of the equation expressing conservation of mass, viz.

$$\frac{\partial[\bar{\omega}]}{\partial p} + \frac{1}{a\cos\phi}\frac{\partial}{\partial\phi}\left([\bar{v}]\cos\phi\right) = 0 \qquad (1)$$

where $\omega = \frac{dp}{dt}$, from which it is seen that calculations of the vertically integrated northward mass flux

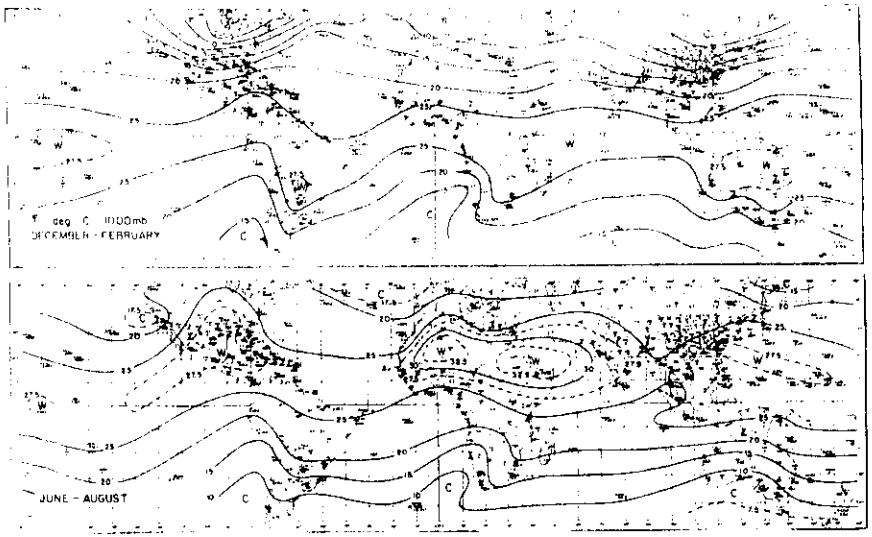

Figure 1

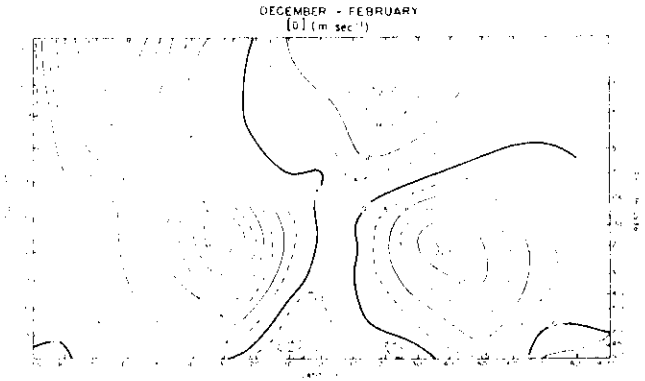

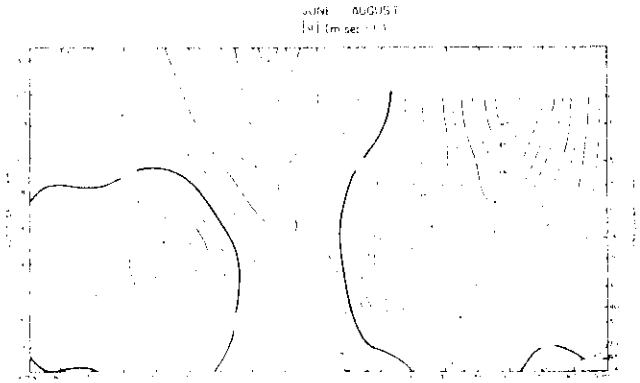

Figure 2

$$\psi(\phi,p) = -\frac{2\pi a\cos\phi}{g}\int_{p}^{p_0}[\bar{v}]\,dp \qquad (2)$$

enables $[\bar{\omega}]$ to be obtained as

$$[\bar{\omega}] = -\frac{g}{2\pi a^2\cos\phi}\frac{\partial\psi}{\partial\phi} \quad . \qquad (3)$$

The mean meridional motion fields for the four seasons obtained by NKVB are shown as curves ψ = const. in Fig. 3. The seasonal variation in strength of the tropical Hadley (direct) cells is well illustrated, together with the poleward excursion of the region of mean ascent between them. Of particular significance for arid regions is the subtropical subsidence, implying moisture export from the subtropics throughout the year.

1.2 The atmospheric heat balance

The atmospheric circulation is driven by differential net heating between the equator and poles. On climatic time scales (longer than a season) local heat storage terms are negligible compared with sources and sinks. The largest net heat input is in low latitudes since the earth's axis makes a relatively small angle with the normal to its orbital plane round the sun and the heat balance there, dictated mainly by radiative cooling, implies a radiative equilibrium temperature there of approximately 250K, assuming an albedo of 35%. At high latitudes the main heat source arises from poleward heat transfer by the eddies, and the simple radiative equilibrium concept is not applicable. The heat balance equation for unit mass of the atmosphere may be written, to a good approximation, as

$$c_p\frac{\partial\bar{T}}{\partial t} = H - c_p\,\bar{\underline{v}}\cdot\bar{\nabla}\bar{T} - c_p\left(\frac{p}{p_0}\right)^{R/c_p}\left\{\bar{\omega}\frac{\partial\bar{\theta}}{\partial p} + \left(\bar{\nabla}\cdot\overline{\underline{v}'\theta'} + \frac{\partial}{\partial p}\,\overline{(\omega'\theta')}\right)\right\} \qquad (4)$$

(i) (ii) (iii) (iv)

Here H denotes the net heating (radiative, latent heat release and boundary layer flux of sensible heat transferred by 'sub-grid-scale' eddies) and θ is the potential temperature $T(p_0/p)^{R/c_p}$ where p_0 is 1000 mb and p is in mb.

Figs. 4(a) and (b) show the zonal mean distributions of H for Dec-Feb and Jun-Aug calculated by NKVB. Both indicate lower tropospheric warming due to surface heat transfer and upper tropospheric cooling. Also evident are the heating maxima in the lower and mid troposphere arising from latent heat release - in the tropics and mid-latitude storm tracks. Figs. 4(c) and (d) show, for comparison, distributions of H obtained at Reading University (RU) using ECMWF archived operational analyses for 1978-84. There are quite

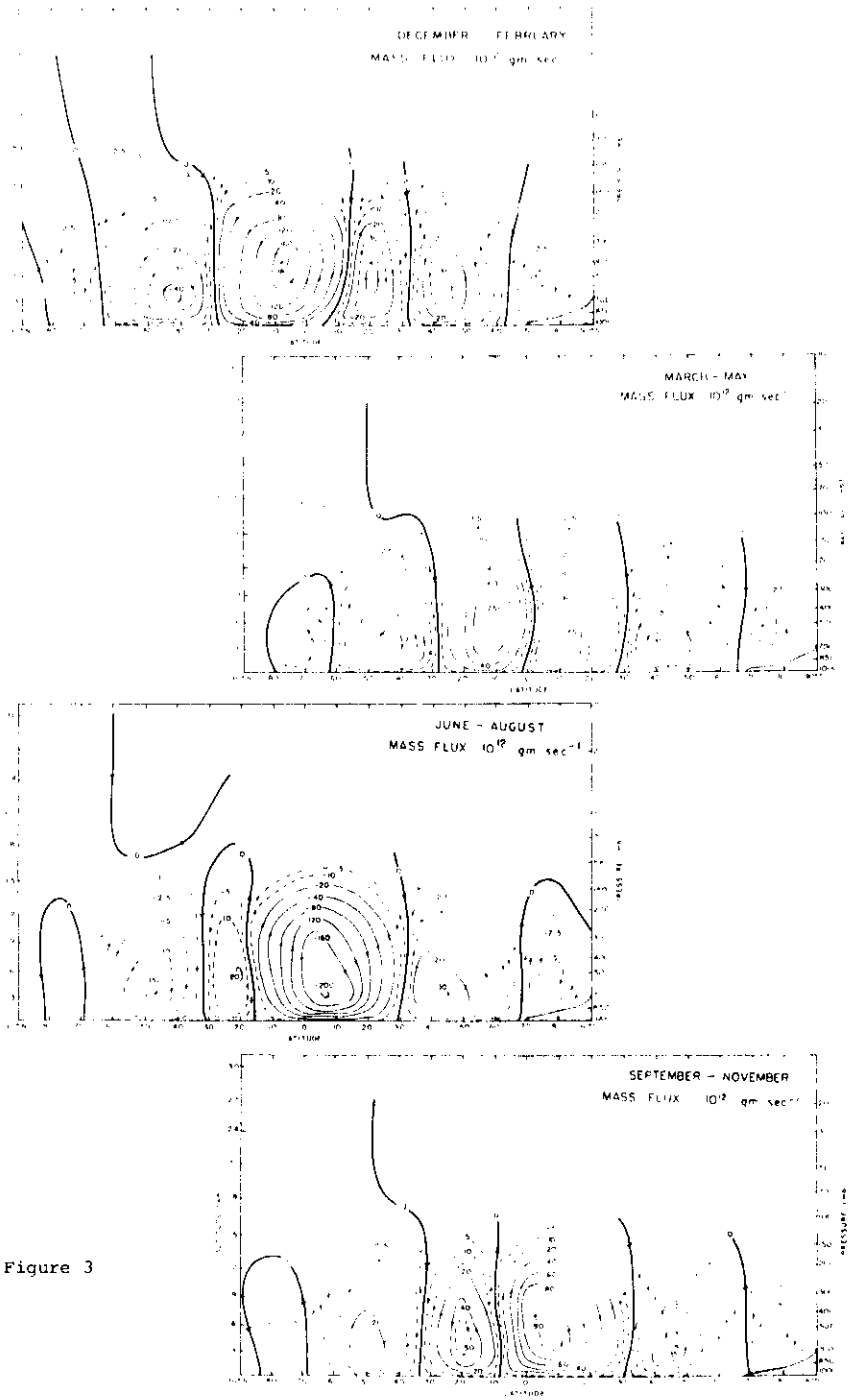

Figure 3

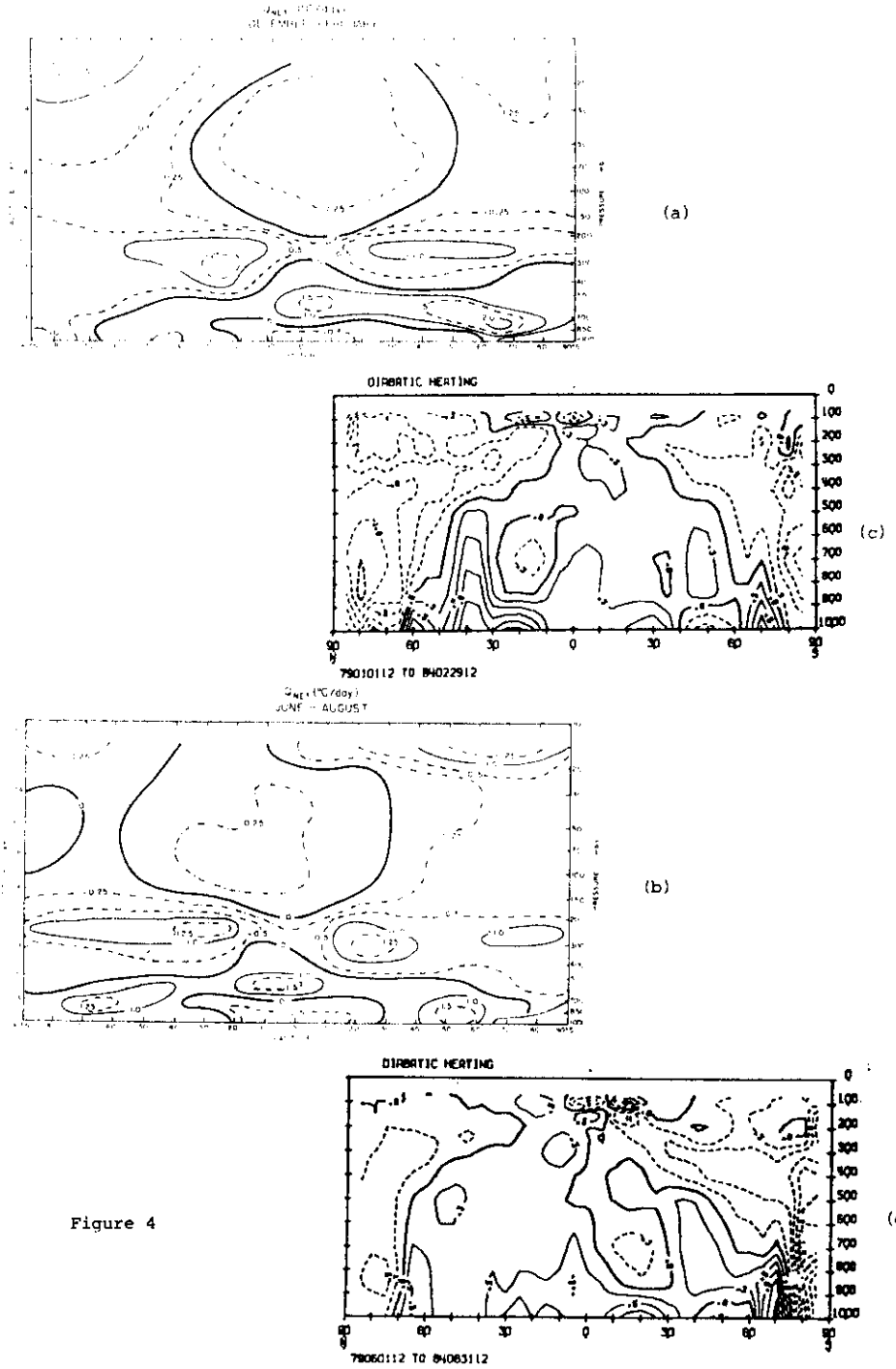

Figure 4

substantial differences from the NKVB estimates, particularly in the mid-latitude troposphere.

Thus, when Eq. (4) is integrated through an atmospheric column, (i) is the net heating, (ii) the steady vertical heat transport, (iii) the steady vertical transport and (iv) the total eddy transport.

Taking the zonal average of (ii) gives

$$\left[c_p \bar{\underline{v}}^* \nabla \bar{T}\right] = \left[\frac{c_p \bar{v}}{a} \frac{\partial \bar{T}}{\partial \phi}\right] = \frac{c_p}{a}\left\{\frac{\partial}{\partial \phi}\,[\bar{v}\bar{T}] - \bar{T}\frac{\partial \bar{v}}{\partial \phi}\right\}.$$

$[\bar{v}\bar{T}]$ is the northward flux of heat and may be expressed as $c_p\{[\bar{v}][\bar{T}] + [\bar{v}^*\bar{T}^*]\}$. RU distributions of the steady eddy temperature flux $[\bar{v}^*\bar{T}^*]$ for Dec-Feb and Jun-Aug are shown in Figs. 5(a) and (b). Zonal means of the transient eddy temperature flux $[\overline{v'T'}]$ are shown in Figs. 6(a)-(d). Those in Figs. (c) and (d) were obtained using a time filter having the effect of including only those eddies with periods of less than about 10 days, e.g. mid-latitude depressions.

The generally poleward transfer of heat by the eddies is clearly seen, mainly concentrated around 800 mb. This is achieved as much (more so in the summer hemisphere) by the low frequency variations of the flow as by the high frequency transients.

The global distributions of (ii), (iii) and (iv) for each season will be considered in detail in Lecture 3.

LECTURE 2 THE GLOBAL ATMOSPHERIC ANGULAR MOMENTUM BALANCE. ZONAL VARIATIONS OF THE CIRCULATION

2.1 The angular momentum balance

A general consistency between the distributions of tropospheric mean zonal wind in Fig. 2 and vertical motion in Fig. 3 is apparent if the effects of surface drag are considered. Thus, for example in the N. Hemisphere, geostrophic control, which is strong poleward of about 10°, implies high mean surface pressure in the subtropics. The effect of surface drag is to reduce the magnitude of the (easterly) surface winds and allow flow down the pressure gradient in the frictional boundary layer. It is thus consistent with the existence of meridional cells in the sense shown in Fig. 3. Even more important in the tropics, however, is the moisture convergence implied by this process and the release of latent heat when it condenses in the region of mean ascent near the equator. This has a fundamental effect on the depth and temperature structure of the troposphere in low latitudes.

Since during a season there is no significant accumulation of atmospheric mass at any latitude, there is a poleward flow in the upper troposphere above the low-latitude easterlies. This air, in the absence of some dissipating or exporting process, would conserve its absolute angular momentum, $[\bar{M}]$. This would imply a mean zonal wind $[\bar{u}]$ of about 130 m s^{-1} at 30° latitude, as is

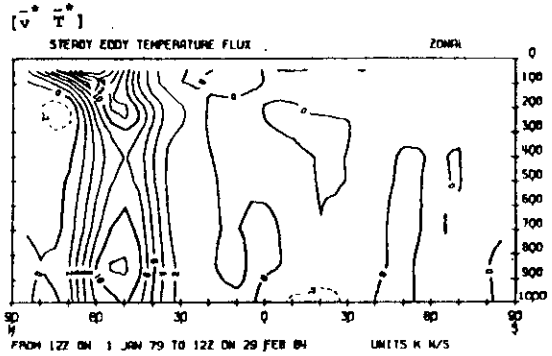

(a)

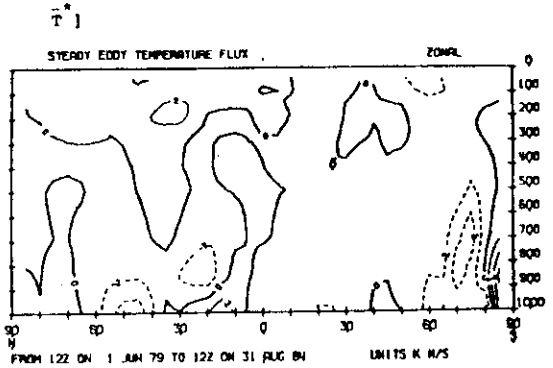

(b)

Figure 5

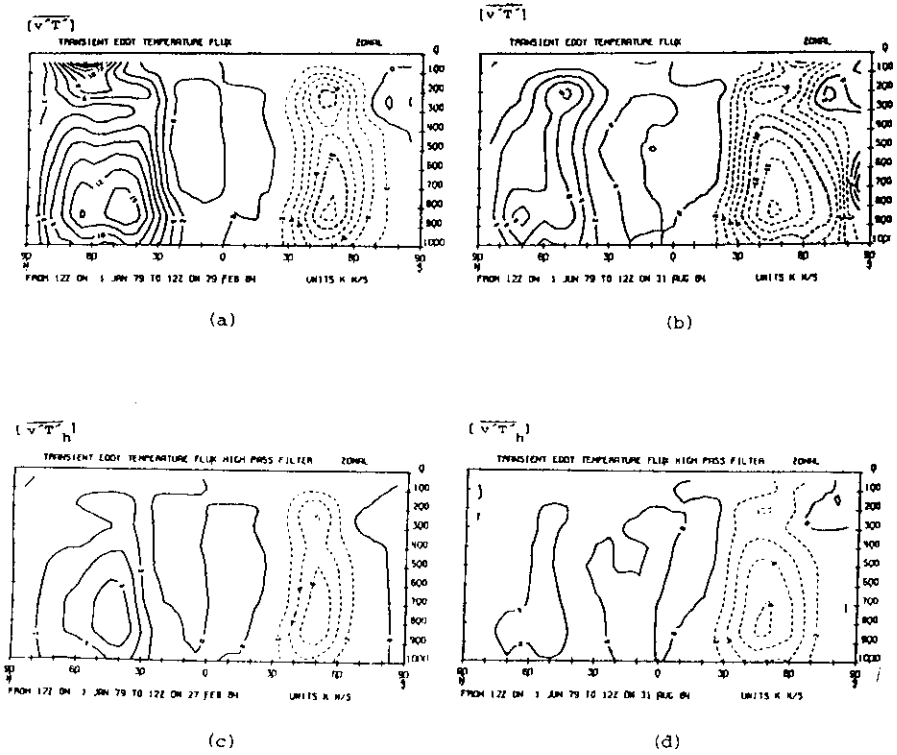

Figure 6

easily shown by writing

$$[\bar{M}] = (\Omega\, a \cos\phi + [\bar{u}])a\cos\phi \quad , \tag{5}$$

where a is the earth's mean radius (6350 km approx.) and Ω its angular velocity, and taking $[\bar{u}] = 0$ at the equator. This would also imply a very large vertical shear and, to satisfy the thermal wind equation, a large horizontal temperature gradient.

If one envisages the setting up of such a flow in, say, a computer model of the atmosphere, then it would be extremely unstable and any small perturbation would result in rapid amplification of wave-like disturbances. It is therefore not surprising that such disturbances, or eddies, occur in the atmosphere, many of them transient, e.g. mid-latitude depressions and tropical cyclones. Others, the so-called planetary waves, are permanent and vary only slowly in amplitude and phase; these have a significant influence on the location of the main climatic zones. Both types of eddy play a fundamental role in the atmospheric angular momentum (a.a.m.) balance and, as was seen in Lecture 1, the heat balance. Thus, for example, the transient waves accomplish a major part of the angular momentum transport in the upper troposphere away from the subtropics, i.e. tend to reduce $[\bar{u}]$ there.

These processes are described by the equation

$$\frac{\partial [\bar{M}]}{\partial t} = -\frac{1}{a\cos\phi}\frac{\partial}{\partial\phi}(\overline{J_\phi}\cos\phi) + \frac{\partial}{\partial p}(\overline{J_p}) - \left[\frac{\partial \bar{\Phi}}{\partial \lambda}\right] \tag{6}$$

where $\overline{J_\phi} = a^2\,\Omega\bar{v}\cos^2\phi + (\bar{u}\bar{v} + \overline{u^*v^*})a\cos\phi$, the horizontal a.a.m. transport, (7)

and $\overline{J_p} = a^2\,\Omega\bar{\omega}\cos^2\phi + (\bar{u}\bar{\omega} + \overline{u^*\omega^*})a\cos\phi + ag\bar{\tau}_\lambda$, the vertical a.a.m. transport. (8)

Here Φ denotes the geopotential of isobaric surfaces, gz, and τ_λ the zonal component of the surface drag.

The zonally averaged, vertically integrated eddy transports for Dec-Feb and Jun-August calculated by NKVB are shown in Fig. 7. These show the tendency of the mean motion (Hadley Cells) to concentrate angular momentum in the subtropics and for the eddies to deplete the tropics of angular momentum and concentrate it in mid-latitudes, where it is removed by surface friction in the westerlies and by mountain drag. The low-latitude surface easterlies are associated with an angular momentum source.

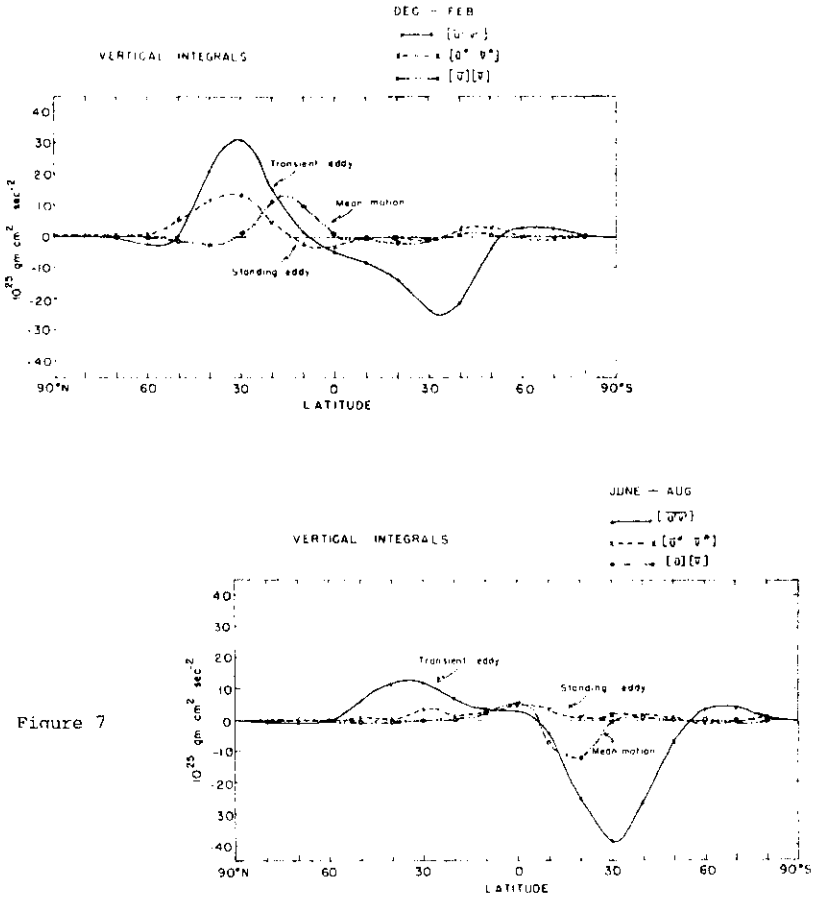

Figure 7

Figs. 8 show distributions of the eddy momentum flux calculated at UR for 1978-84. As in the case of the heat flux, this is dominated by the transient eddies. The main transfer, however, takes place in the upper troposphere near the subtropical jets - not surprising in view of the large value of $[\bar{u}]$ there. The higher frequency eddies generally contribute less than the lower frequency variations; numerical experiments on the life-cycles of baroclinic waves show that it is only in their decaying stages that poleward momentum transfer occurs and then mainly at upper levels (the poleward heat transfer occurs mainly in the amplifying stage and tails off as the systems occlude). The patterns clearly show that the eddies tend

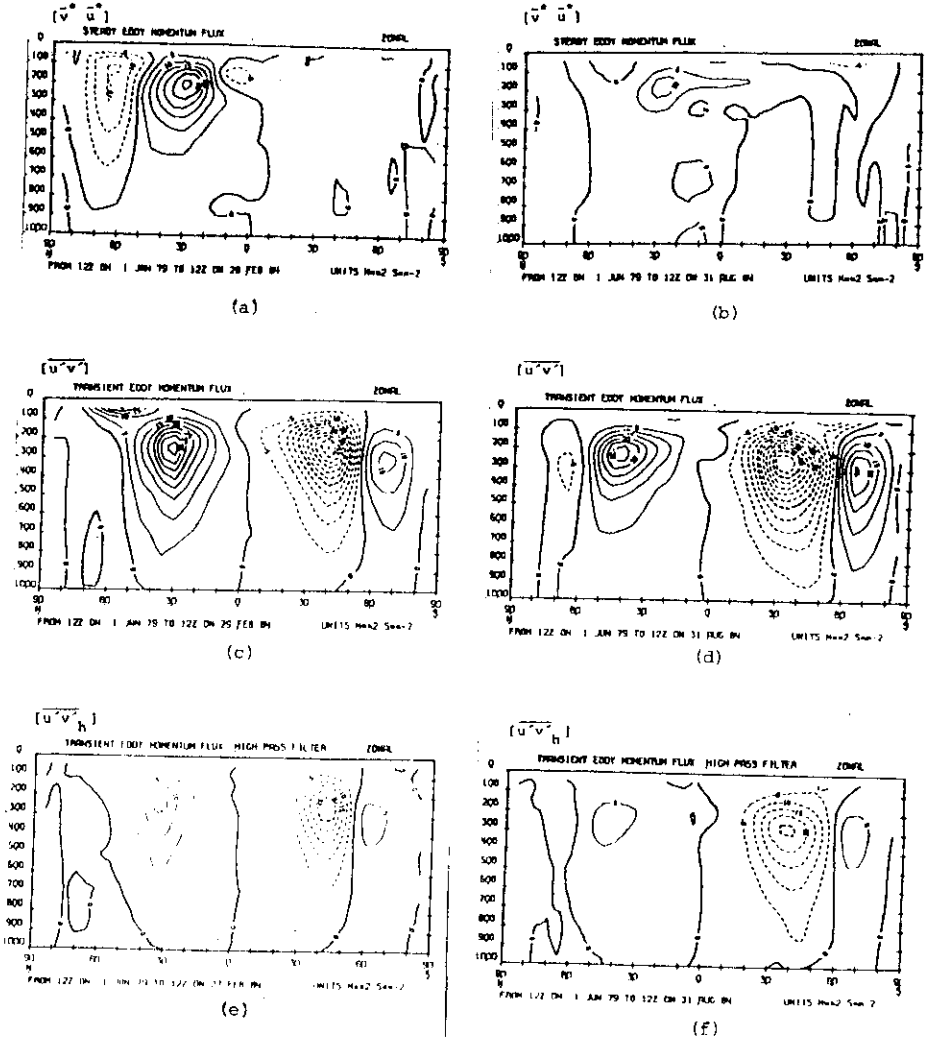

Figure 8

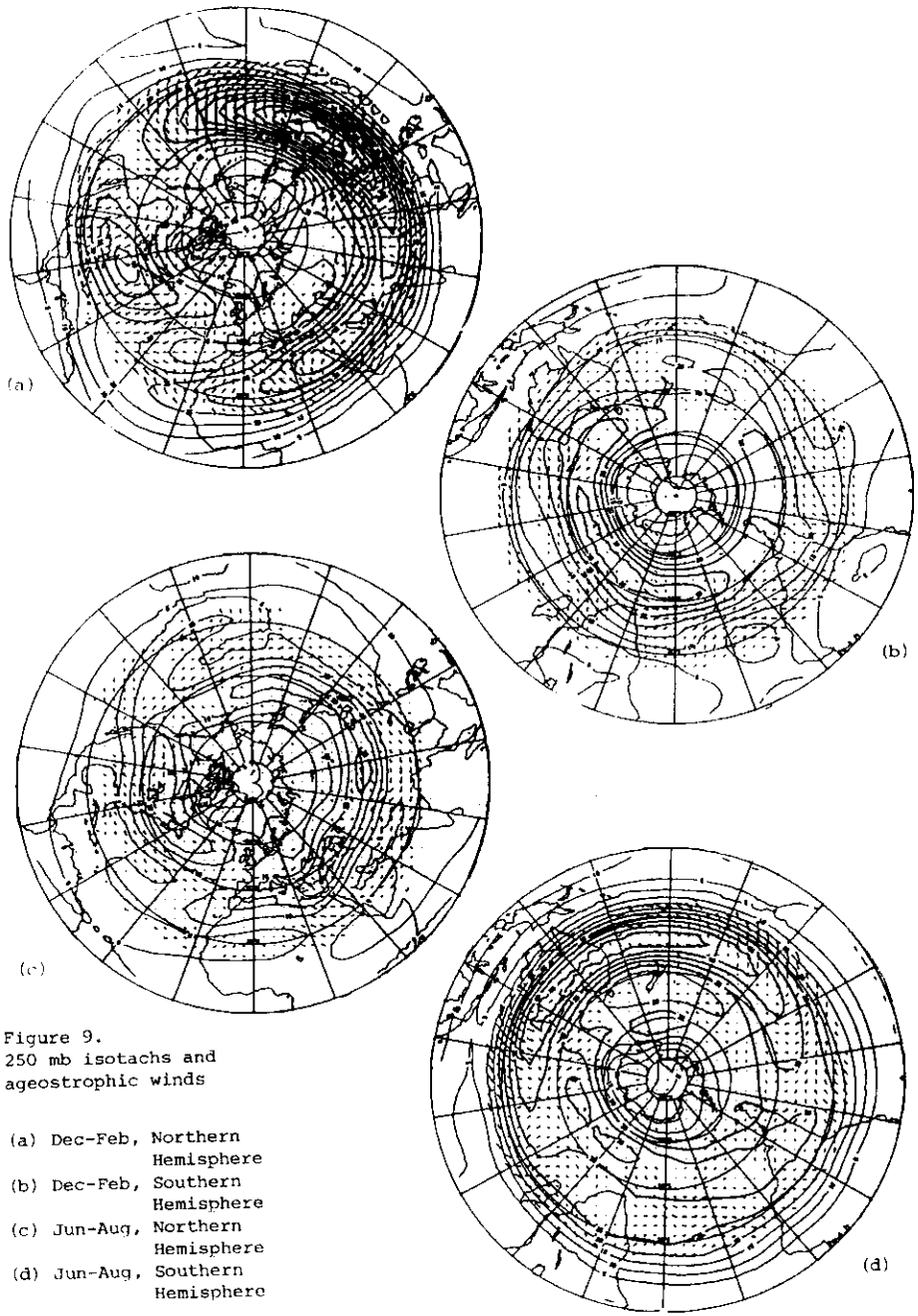

Figure 9.
250 mb isotachs and ageostrophic winds

(a) Dec-Feb, Northern Hemisphere
(b) Dec-Feb, Southern Hemisphere
(c) Jun-Aug, Northern Hemisphere
(d) Jun-Aug, Southern Hemisphere

to reduce $[\bar{u}]$ in the subtropical jet and increase it further polewards. As has already been pointed out, the mean poleward motion in the upper branch of the Hadley cell implies increasing $[\bar{u}]$ following fluid elements and thus the strength of the jet is determined by the balance between these two factors. In an analogous way, polewards of the jet the tendency of the eddies to increase $[\bar{u}]$ is offset by a mean meridional equatorwards flow in which angular momentum tends to be conserved; this is part of the mechanism of the mid-latitude Ferrel (indirect) cell; the other component is the polewards (down the pressure-gradient) flow in the boundary layer westerlies.

2.2 Zonal variability of the seasonal mean flow

Considerations of the zonal mean flow and the angular momentum balance have highlighted the upper troposphere as the region where the eddies have their strongest influence on the mean flow. This is borne out by the distributions of mean wind speed $|\underline{v}|$ and ageostrophic motion $\underline{v}_a$ at 250 mb for Dec-Feb and Jan-Aug shown in Fig. 9. The winter hemispheres show striking zonal variations in $|\underline{v}|$, from 15 m s^{-1} to 65 m s^{-1} in the northern hemisphere and 25 m s^{-1} to 45 m s^{-1} in the southern hemisphere.

Clearly the large mountain masses of the planet (Himalayas, Rockies, Greenland and Antarctica) play a role in determining these asymmetries; but so also do the main tropical heat sources. Idealised numerical experiments have been carried out by Grose and Hoskins (JAS 1979, pp 223-234) and Hoskins and Karoly (JAS 1981, pp 1179-1196), in which the perturbations of a purely zonal flow, resembling the climatological mean, produced by mountain masses and large-scale heat sources were studied. Two such results are shown in Figs. 10(b) and (c); Fig. 10(a) shows the observed mean climatological 200 mb stationary wave height field for comparison.

All three patterns exhibit trains of stationary Rossby waves. Those generated by the mountains (Fig. 10(b)) strongly resemble those observed, at any rate in their phases; however the computed amplitudes are only about $\frac{1}{3}$ of those observed. The waves generated by the single subtropical heat source display two interesting propagating components, one round a great circle and the other zonal. The amplitudes involved are comparable with those observed if the heat source is assumed to be of the observed climatological value of the Indonesian source (approximately 200 W m^{-2} maximum).

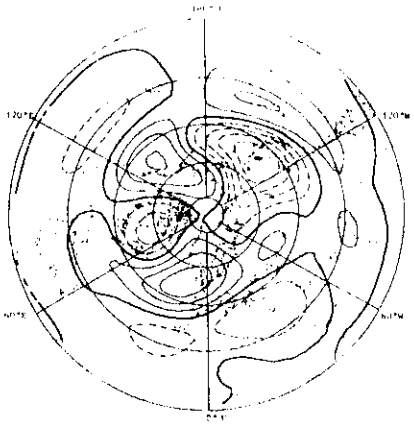

(a)

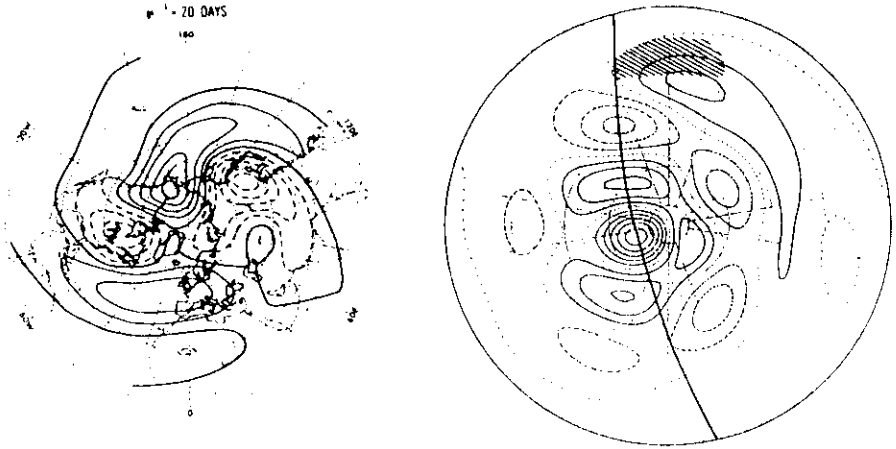

(b) (c)

Figure 10

Planetary wave perturbations

(a) 200 mb observed
(b) model mountain forcing
(c) model tropical heat source.

(See text for details.)

LECTURE 3 ARID REGIONS AND THE ZONAL VARIABILITY OF THE GLOBAL CIRCULATION

In the last lecture the roles of mountain ranges and tropical heat sources in generating zonal asymmetries were discussed using the results from idealised numerical experiments. The planetary waves arising from the simulated mountains were adiabatic - no heat sources being included in the model - so that the balance in the thermal energy equation (4) in the steady state configuration is between terms (ii) and (iii), i.e. horizontal and vertical advection by the mean flow. With the tropical heat source included there is also a contribution from the heating term (i) in the steady state.

3.1 Arid zones in the general circulation

The maintenance of an extensive arid zone requires the atmosphere over the region to be continually subsiding. This is seen by considering the moisture balance equation in pressure coordinates

$$\frac{\partial q}{\partial t} + \nabla \cdot (\underline{v}q) + \frac{\partial}{\partial p}(\omega q) = E - C \qquad (9)$$

where q denotes the specific humidity, E the evaporation rate and C the condensation rate per unit mass of air. Integrated through a vertical column this becomes, for the steady state,

$$\int_0^{p_s} q\nabla\cdot\underline{v}\,\frac{dp}{g} + \int_0^{p_s} \underline{v}\cdot\nabla q\,\frac{dp}{g} = E_s + \int_0^{p_s} (E - C)\,\frac{dp}{g} \quad , \qquad (10)$$

where suffix s denotes a surface value. For an arid region the integral involving E - C is zero, i.e. the only evaporation involved is from the surface. Also when the terms on the left of (10) are integrated over a large isolated land or ocean area the first term strongly dominates, because in lower latitudes the heating contrast between a large land mass and the surrounding ocean tends to set up a circulatory low-level wind system centred over the area, rather than allow a general flow across it. Thus, with $E_s > 0$, $\nabla\cdot\underline{v}$ must be positively correlated with q to satisfy Eq. (10), i.e. since $\frac{\partial q}{\partial p} > 0$, $\nabla\cdot\underline{v}$ must be positive at low-levels. This implies general subsidence over the region. [The reverse applies, of course, when C > E and the RHS of Eq. (10) is negative.] When the subsidence occurs over the sea, the problem of aridity does not arise since there is an ample moisture source; over land, however, drying out occurs when subsidence persists.

The factors which determined the location of the main regions of large-scale subsidence in the global circulation must therefore be identified if the factors which determine the location of the main arid zones are to be understood.

3.2 The main features of the global climatology for 1978-84

Although climatological fields have been analysed for all four seasons, only those for Dec-Feb and Jun-Aug are presented here. Figures 11 and 12 show upper and lower level winds and net tropospheric heating over the tropical belt for these seasons.

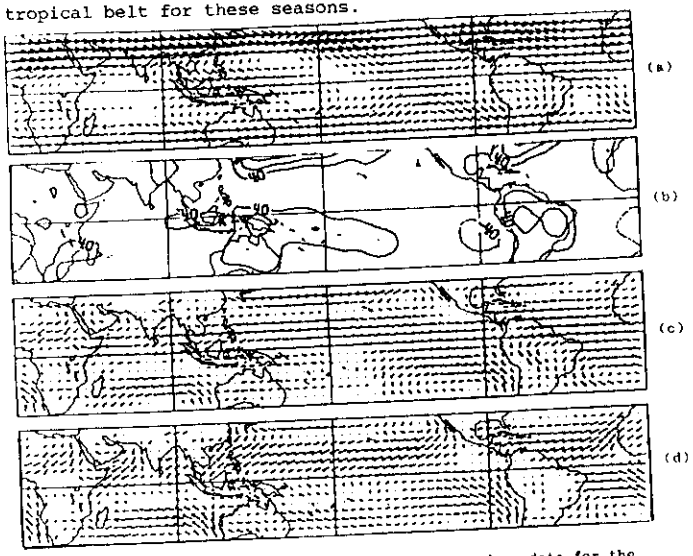

Figure 11 Mean winds during December-February, based on data for the years 1979-84, between 35°S and 35°N at (a) 150, (c) 850 and (d) 1000 mb. A 3mm long arrow corresponds to a wind speed of 27 m s^{-1} in (a), and 13.5 m s^{-1} in (c) and (d). The pattern of large-scale, vertically integrated diabatic heating is shown in (b). The contour interval is 40 Watts/m^2; heating is indicated by solid and cooling by dashed contours. The zero contour is not shown for clarity. The field has been smoothed prior to plotting with an isotropic filter that effectively retains length scales up to spherical wavenumber n = 24.

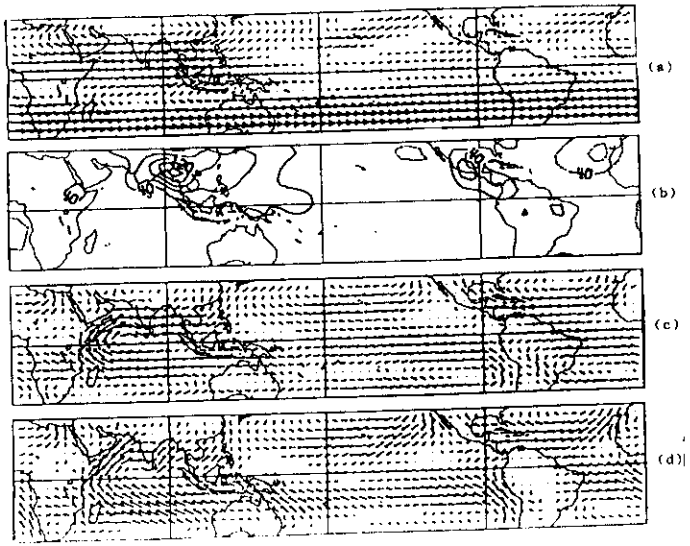

Figure 12

As in Fig. 11, but for June-August.

The wind distributions are well known. For Dec-Feb (DJF) the subtropical jets at 150 mb are both evident together with tropical easterlies over the W. Pacific and Atlantic and westerlies over the E. Pacific. In the lower troposphere easterlies are present over most of the tropical belt linked to the subtropical anticyclonic gyres. The cross-equatorial W. Pacific winter monsoon flow is also apparent. The heating distribution has its low-latitude maxima over Indonesia, S. America and E. Africa; also evident are the heating regions associated with the N. Hemisphere mid-latitude oceanic storm-tracks. The northward shift of the sub-tropical jets in Jun-Aug (JJA) is clearly evident in Fig.12; so also are the Asian monsoonal winds at both upper and lower levels - and the disappearance of the E. Pacific upper equatorial westerlies. The spectacular north-westward shift of the main heating region from the equator to about 20°N over N.E. India and, to a lesser extent, the displacement of the American and African heat sources is also shown. However, no S. Hemisphere storm track heat sources are evident.

These figures enable one to attach an upper level flow signature to the major tropical heat sources - a pair of anticyclonic gyres, one each side of the equator. These are associated with the upper level outflow from the deep convective systems in which latent heat is released.

There is a significant difference between the nature of the thermal balances in the tropics and latitudes poleward of about 20°. Whereas in the tropics the dominating balance is between latent heat and vertical transport, at higher latitudes horizontal transport by the mean flow plays an equally important role; the eddies are by no means entirely negligible, but generally play a role which is minor relative to the other factors. These characteristics are clearly seen in Figures 13 and 14 showing DJF and JJA fields of the total heating and steady horizontal transport terms in the thermal balance equation; this may be expressed as

$$\text{Net heating} = \text{steady vertical transport } \left(\bar{\omega}\frac{\partial\bar{\theta}}{\partial p}\right) + \text{steady horizontal transport } (\bar{\underline{v}}\cdot\nabla\bar{\theta})$$

$$+ \text{transient eddy transport } \left(\overline{\omega'\frac{\partial\theta'}{\partial p}} + \overline{\underline{v}'\cdot\nabla\theta'}\right) , \qquad (11)$$

the storage term being ignored. Thus, for example, positive contours of $\bar{\omega}\frac{\partial\bar{\theta}}{\partial p}$ correspond to ascent. Figures 13(a) and (b) show the tropical heating (Fig. 11(b) in a global context) with the main tropical heating in the S. Hemisphere; virtually all of this heating equatorwards of 20°S is offset by mean ascent (Figure 13(d)), there being virtually no contribution from horizontal advection (Figure 13 (f)) in the mean flow or from eddies (Figure 13(h)). On the other hand, in higher latitudes, the contribution from mean flow horizontal

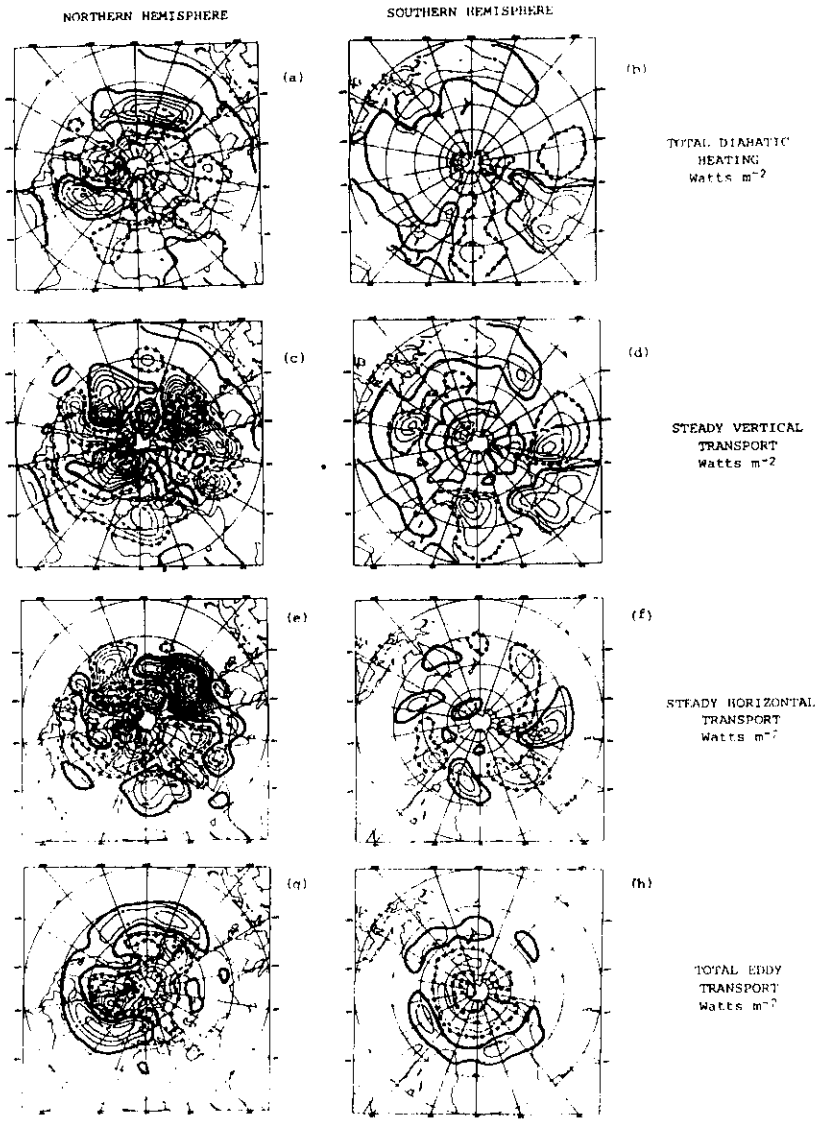

Figure 13. DJF components of the thermal energy equation (Eq. (11)), calculated from ECMWF data, with the latent heating as a residual, for 1978-84. Contour interval 50 W m^{-2}, negative values dashed. -50 W m^{-2} contour dotted; +50 W m^{-2} thick full line.

advection is large, largely offsetting the vertical advection. The eddy contribution is appreciable from about 30° polewards and clearly indicates the role of the mid-latitude eddies transferring heat polewards, tending to cool the subtropics and warm the poles. The N. Hemisphere storm tracks are particularly well marked, as is the much more extensive, almost zonally symmetric, storm track region of the S. Hemisphere.

The JJA heating, dominated by the Asian monsoon source, shows similar stationary planetary wave characteristics (Figures 14(a),(b)). The large, almost cancelling, contributions from the steady vertical and horizontal transport terms over the net heating from the storm track regions are smaller than in DJF even in the S. Hemisphere.

The wave-like structure of the heat transports by the horizontal and vertical components of the mean flow and their large cancelling component suggests a useful partitioning of the steady vertical transport. Writing (11) as

$$-\text{Steady vertical transport} = -\text{Net heating} + \text{steady horizontal transport} + \text{transient eddy transport},$$

the steady vertical heat transport may be partitioned into three components:

(i) a part which just balances the net heating, referred to as the diabatic component,

(ii) a part just offsetting the horizontal advection by the mean flow, referred to as the adiabatic planetary wave component, and

(iii) a part just balancing the transient wave source, referred to as the transient wave component.

Since (iii) is of a magnitude comparable with (i) and (ii) only in latitudes polewards of about 30°, the climate of the tropics and subtropics, mainly determined by the steady vertical motion, is analysed here only in terms of (i) and (ii), i.e. is partitioned into an adiabatic component and a diabatic component. [Such a partition is not appropriate to higher latitudes since the transient waves cannot be regarded as adiabatic.]

Thus, for example, the distribution of steady vertical transport with the sign reversed in Fig. 13(c) between about 35°N and 35°S (positive values indicating ascent) may be regarded as the sum of the diabatic component (Fig. 13(a)) and an adiabatic planetary wave component (the signs reversed). However, it must be stressed that there is no implication in this partitioning that the components are independent. On the contrary, they are closely related.

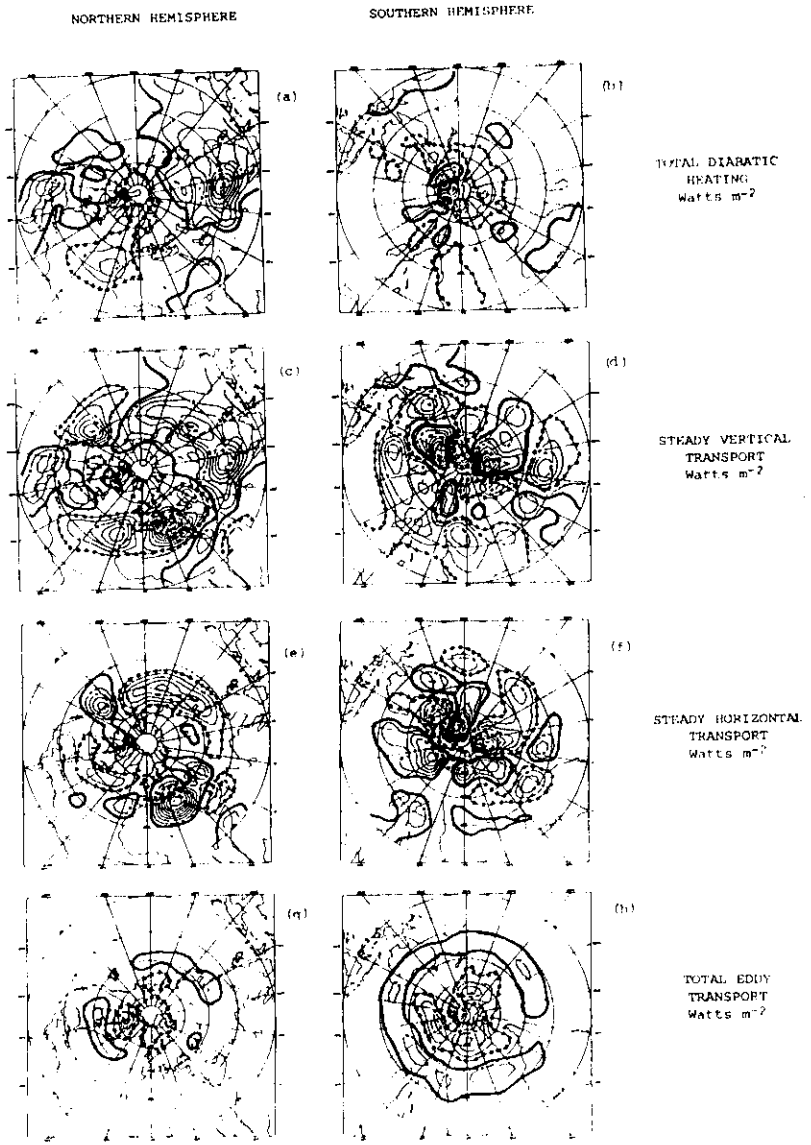

Figure 14. As Figure 13 but for JJA.

The results of partitioning the vertical motion distribution in this way are summarised in Table 1.

TABLE 1

VERTICAL MOTION CLIMATOLOGY - SUMMARY

ASCENT

	N. HEMISPHERE	S. HEMISPHERE
DEC - FEB	PACIFIC, ATLANTIC (STORM TRACKS)	*W. PACIFIC, AUSTRALIA S. AMERICA E. AFRICA*
JUN - AUG	*S. ASIA, W. PACIFIC CENTRAL AMERICA CENTRAL AFRICA*	

SUBSIDENCE

	N. HEMISPHERE	S. HEMISPHERE
DEC - FEB	E. ATLANTIC, N.AFRICA E. ASIA, W. PACIFIC E. U.S.	E. ATLANTIC E. PACIFIC S.E. INDIAN OCEAN
JUN - AUG	E. ATLANTIC, N.AFRICA E. PACIFIC	E. ATLANTIC INDIAN OCEAN

THIS TYPEFACE INDICATES DOMINANT HEATING COMPONENT

THIS TYPEFACE INDICATES SUBSTANTIAL PLANETARY WAVE COMPONENT

LECTURE 4 INTERANNUAL VARIABILITY OF THE GLOBAL CIRCULATION - ANOMALIES FOR 1983, 1984. THEORETICAL CONSIDERATIONS

It is well known that rainfall in arid regions may be highly variable from year to year (see, e.g., Fig. 19 of 'The Global Climate System' referring to S.E. Africa), and that such regions may be subject to periods of prolonged drought. A fundamental question which arises is to what extent this variability is dictated by the large-scale dynamics of the entire atmospheric circulation and to what extent, if any, by purely local features, e.g. changes in albedo due to changing vegetation. We are now able to estimate, with a fair degree of accuracy, the global distribution of atmospheric heat sources and sinks for each season each year and thus obtain an estimate of the heat source and sink seasonal anomalies. [Seasonal mean flow anomalies have been available for many years.] These are now discussed and related to the heating anomalies for 1983 and 1984.

4.1 December-February

These are shown in Figure 15. The most striking feature is the large upper anticyclone anomaly pair at 150 mb over the central Pacific during the El-Niño event of 1982/3 followed in 1983/4 by an anomaly of the opposite sign (Figs. 15 (a) and (b)). In 1982/3 the climatological E. Pacific equatorial westerlies (Fig. 11(a)) almost disappear. The change in sign of the mid-Pacific equatorial 850 mb winds from westerly to easterly is no less dramatic Figs. 15(e) and (f)). The anomalous heating extends from the Indian Ocean right across the tropical Pacific but, although large in extent, does not much exceed 40 W m^{-2}. This is surprising in view of the strong anomalous 150 mb anticyclonic gyres, on each side of the equator; the heating anomaly is not only weak, it is also concentrated mainly in the southern hemisphere. It is clear too that 1983/4 was strongly anomalous in the Indian Ocean with stronger than normal upper easterlies across the whole belt from 20°S to 20°N extending across Africa and low-level westerlies near the equator. This is clearly associated with a strong anomalous heating of up to 120 W m^{-2} over Indonesia. Also of interest is the large area of increased cooling over much of the central and eastern Pacific, in contrast to a heating anomaly there in 1982/3.

Thus although the 1982/3 El Niño has been much highlighted, the evidence provided by these anomaly patterns suggests that 1983/4 was, in its way, equally dramatic. In both seasons the heat source over S. America is appreciably larger than normal.

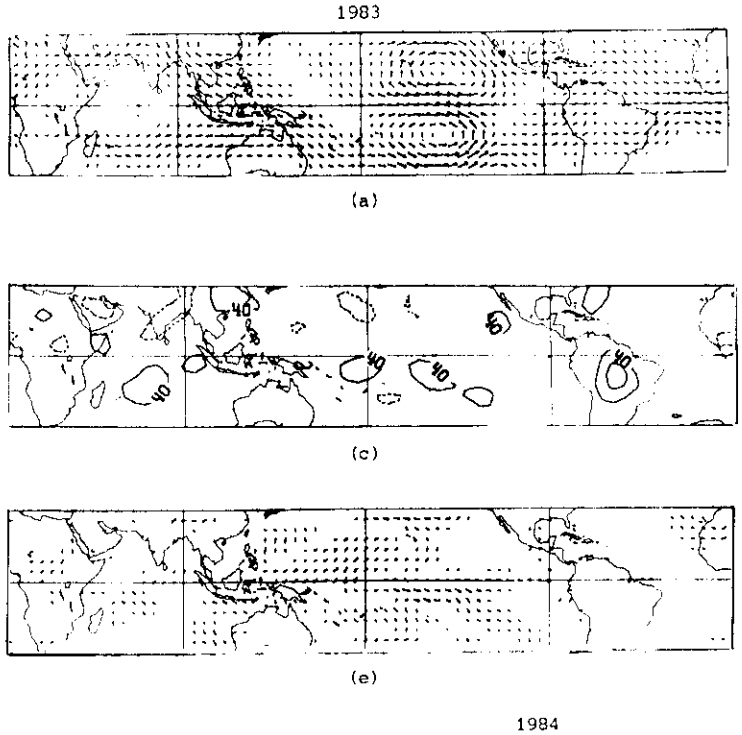

Figure 15.

DJF anomaly winds at 150mb for (a) 1983, (b) 1984 and 850mb (e) 1983, (f) 1984 based on 1978-84 Climatology (Figs.11,12) and anomaly heating distributions (c) 1983 and (d) 1984. Format as for Fig. 11.

4.2 June-August

These anomalies are shown in Fig. 16. Strengthened upper westerlies over the Indonesian region in 1983 and, to a lesser extent, in 1984, and upper easterlies over Africa in 1984 are the main features at upper levels. Both years are characterised by strengthened easterlies at low levels over the central and W. equatorial Pacific, and in 1984 there is some slight strengthening of the Asian monsoon westerlies. These low-level winds are consistent with low-level convergence into the main heating anomaly regions. In 1984 there is a strong asymmetry in the heating anomalies between the two hemispheres, heating in the N. Hemisphere and cooling in the S. Hemisphere as, indeed, there is in 1983 also.

The presentation of the anomalies of the thermal energy balance components follows a format slightly different from that of Figures 13 and 14 so that the anomaly steady vertical transport with its sign changed (diagrams (a) and (b)) can be seen as a sum of the diabatic component ((c) and (d)) and the adiabatic component ((e) and (f)); (g) and (h) show the anomaly eddy transport.

An analysis of the various components of the thermal energy equation (Eq. (4)) has also been carried out for the anomaly fields (see Pearce, 1985 - WMO/WCRP Publication No. - Papers presented at the First WMO Workshop on the diagnosis and prediction of monthly and seasonal atmospheric variations over the globe 29 July - 2 August 1985, College Park, Maryland, USA). The main features are

(a) the large magnitudes of the heating anomalies in the tropics - of the same order of magnitude as the seasonal mean,

(b) the large contribution of the planetary wave component in the subtropics tending to reinforce the heating component, and

(c) the relatively minor contribution of the eddy anomalies.

4.3 Linear theory of the tropical circulation

The basic foundations of the theory of the flow associated with tropical heat sources and sinks were laid by Matsuno (1966, Journal of the Meteorological Society of Japan, pp 25-43). He carried out an analysis based on the shallow water equations on an equatorial beta-plane, linearised about zero mean flow, and showed that the free modes in a two-layer system comprised (a) an eastward propagating Kelvin wave, (b) a westward propagating Rossby-gravity wave and (c) eastward and westward propagating gravity-inertial waves.

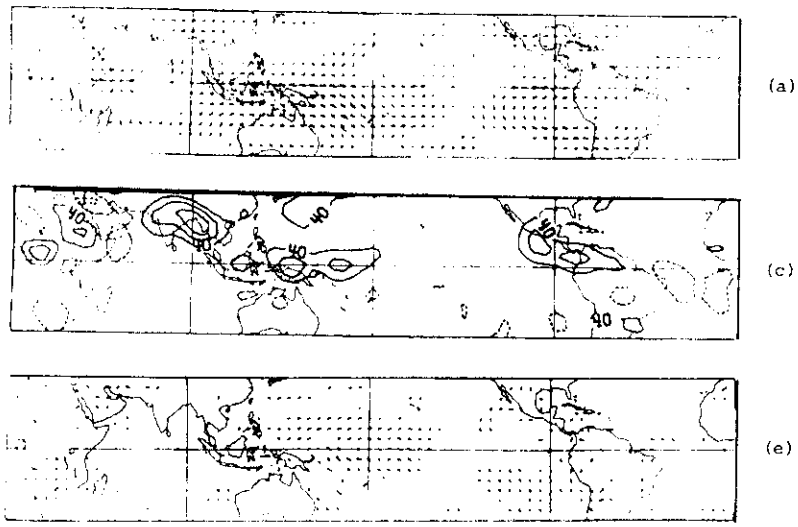

1984

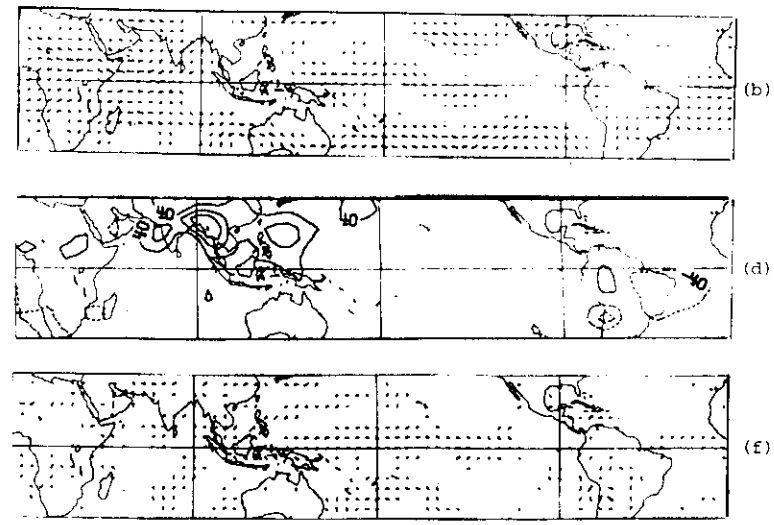

Figure 16.

As Fig. 15 but for JJA.

The forced steady state corresponding to a tropical heat source of continental dimensions comprises primarily of components (a) and (b). Schematic diagrams of the free mode (propagating) Kelvin and the largest meridional symmetric and asymmetric Rossby waves are shown in Figs. 17. Figs. 18 show an analytical solution for the steady state circulations forced by tropical heat sources, (a) and (b) centred on the equator and (c) and (d) centred at about 20°N; these are due to Gill (1980, Q.J. Roy. Met. Soc., pp 447-462).

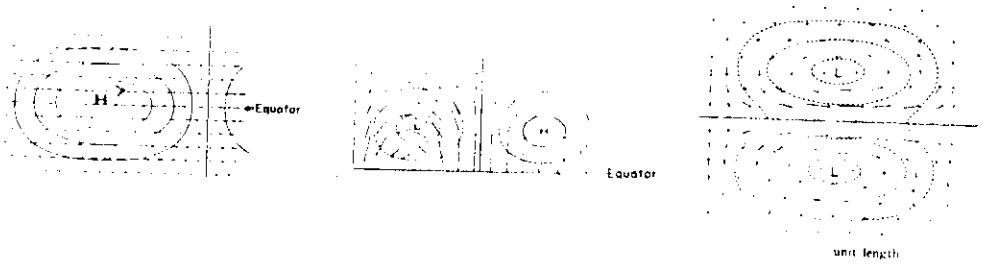

(a) Kelvin (b) Rossby (n = 0) (c) Rossby (n = 1)

Figure 17

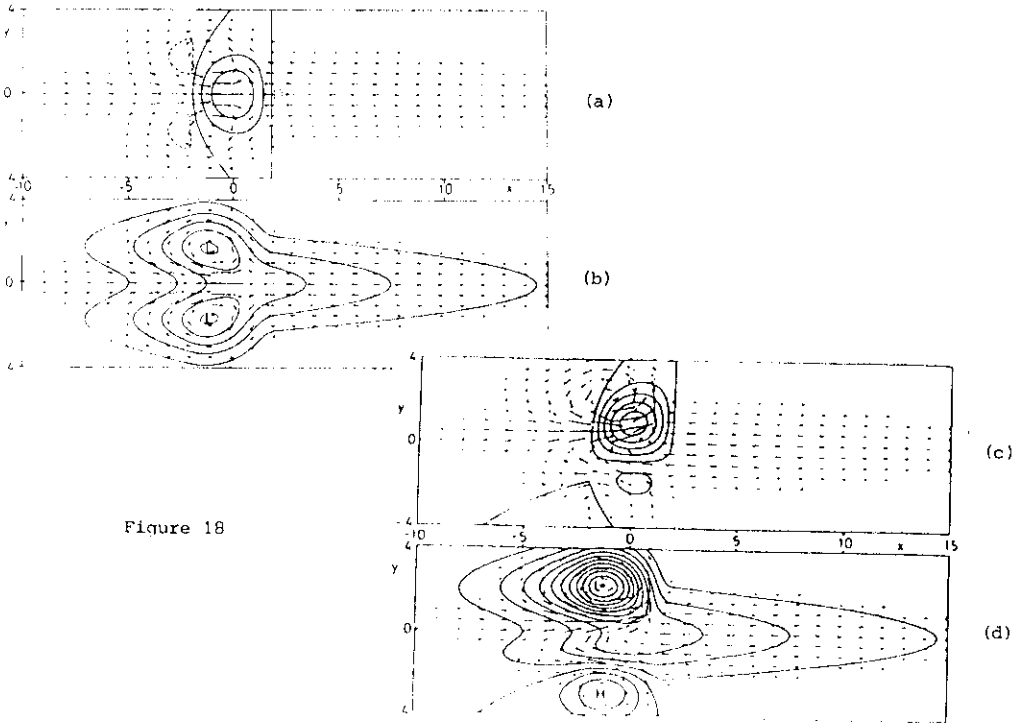

Figure 18

It is useful to compare Gill's asymmetric solution with the JJA climatology over the Asian monsoon region, and this is shown in the schematic representations of the upper and lower tropospheric flow in Fig. 19.

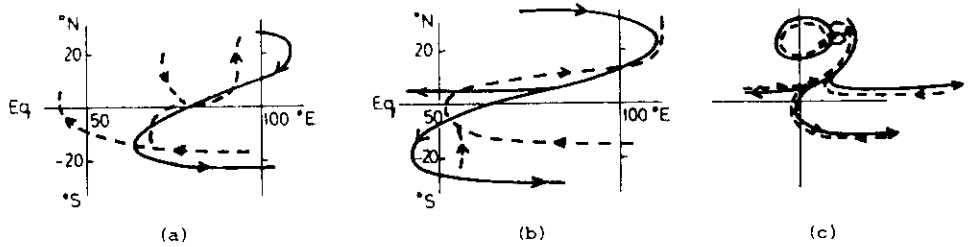

Figure 19

Schematic of mean Asian summer monsoon flow at lower levels (dashed) and upper levels (full line).
(a) May 1979, (b) June 1979, (c) Gill's model (Figs. 18(c), (d))

The similarities are quite striking, although there are important differences of detail, notably the lack of an upper return cross-equatorial flow concentrated directly above the low-level Somali jet. The two-level linearised model does remarkably well both in this case and for the flow over the Indonesian heat source in DJF.

The main limitations of the theory arise from

(a) the neglect of a background zonal mean flow,

(b) the neglect of non-linearities,

(c) the crude vertical structure, and

(d) the representation of dissipative processes.

LECTURE 5 STUDIES OF REGIONAL FEATURES USING NUMERICAL MODELS

5.1 Monsoons

The term 'monsoon' is applied to the rainy season in three main regions of the globe: (a) S. Asia, particularly India (the Asian 'summer' monsoon), (b) Indonesia and N. Australia (the Asian 'winter' monsoon), and (c) W. Africa. In regions (a) and (c), particularly, the economies of vast semi-arid areas are crucially dependent on monsoon rainfall: the ability accurately to predict the monsoon onset and rainfall amount would bring large economic benefits to these regions. These events are clearly associated with the seasonal shifts of the main centres of tropical heating already discussed. As far as the monsoon onset is concerned, deterministic numerical models are just starting to show some promise of predictive skill up to a few days ahead, and considerable effort is being devoted to improving the performance of these models, particularly for the tropics. The nature of these developments is illustrated in Section 5.2.

On the longer time scales, statistically based methods have been extensively developed, e.g. the location of the axis of the 500 mb anticyclone over India in Feb-March has proved to be a useful indication of the seasonal monsoon rainfall over India - the further north it is, the higher the rainfall. There are also good correlations between 'El Niño' events and summer monsoon rainfall (see 'The Global Climate System' pp 29-31). Improvements in these methods are only likely to arise as a result of increased understanding of the physical and dynamical processes involved on longer time scales, for example those involving changes in soil moisture and atmosphere-ocean interaction; the 1982/3 'El Niño' event in the Pacific (see 'The Global Climate System' pp 7-18) is a dramatic recent example of the latter. Such increased understanding can only be acquired through (a) diagnostic studies and (b) experimentation with numerical (and possibly analytical) models.

5.2 The Asian summer monsoon onset

The results of some recent numerical simulations at ECMWF of the 1979 summer monsoon onset are now described to illustrate the present status of numerical prediction for the tropics. The role of moisture is crucial here, with strong dynamical feed-back through latent heat release. Developments occur particularly rapidly over the Arabian Sea and peninsular India during late May and early June. The full curve in Fig. 20(c), showing the time sequence of the KE of the mean 850 mb wind over this region (41.25 - 75 E, 0 - 22.5 N) for May/June 1979 illustrates this.

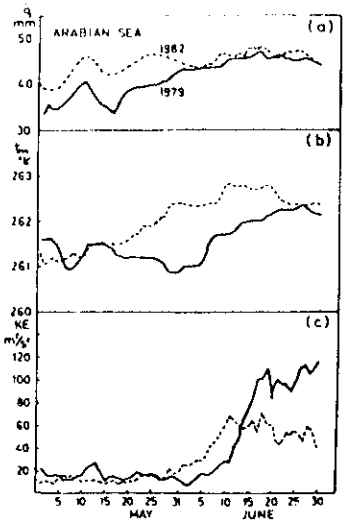

Also apparent in Figure 20 are the increase in moisture during late May and the warming of the atmosphere over the region as the latent heat release occurs.

Figure 20

(see text)

The ECMWF model simulations (see ECMWF Tech. Note No. 44) used as initial data analysed and initialised fields for 1200Z, 11 June 1979, and the investigations were carried out on the 15-level operational grid-point model ($\Delta\lambda = \Delta\phi = 1.875°$). One simulation used a convective parameterisation based on Kuo's scheme while the other used Arakawa and Schubert's (A-S) scheme.

The basic assumption in Kuo's scheme (Kuo, 1965, 1974) is that cumulus convection occurs in layers of conditionally unstable stratification and is maintained by the moisture supply due to large-scale convergence and evaporation from the surface. The environment is convectively heated and moistened by lateral mixing of cloud and environmental air, the amount depending on the local temperature and moisture excess of the cloud ascent over the environment. The net column heating and moistening is assumed to be in equilibrium with the net moisture supply by large-scale convergence and surface evaporation. The Kuo-scheme used in this study is identical to that used in the ECMWF operational forecast model (Tiedtke et al., 1979).

The scheme proposed by Arakawa and Schubert (1974) is one of the most comprehensive cumulus parameterisation schemes. It is based on a theory which describes the interaction of a cumulus cloud ensemble with the large-scale environment. Heating and moistening of the environment is through cumulus induced subsidence and detrainment of saturated air at cloud tops.

The cloud mass flux is determined by the closure assumption that the generation of the cloud available potential energy by the large-scale flow is in quasi-equilibrium with its destruction due to clouds. The scheme used in this study is described in detail by Tiedtke (1985). It has been developed by closely following the original proposal by Arakawa and Schubert, and as further outlined by Lord et al. (1982); the exception is in the cloud physics where we simply assume that cloud water is instantaneously converted to precipitable water, which then detrains at the cloud tops, and that rain re-evaporates in sub-cloud layers as well as within the environmental air of cloud layers. The re-evaporation of rain in cloudy layers signficantly reduces the scheme's tendency to cause excessive drying of the atmosphere as noted by Lord (1982). Cumulus scale transport of horizontal momentum is disregarded in both schemes.

The resulting time sequences of total moisture, tropospheric mean temperature and KE per unit mass of the 850 mb flow over the Arabian Sea are shown in Fig. 21.

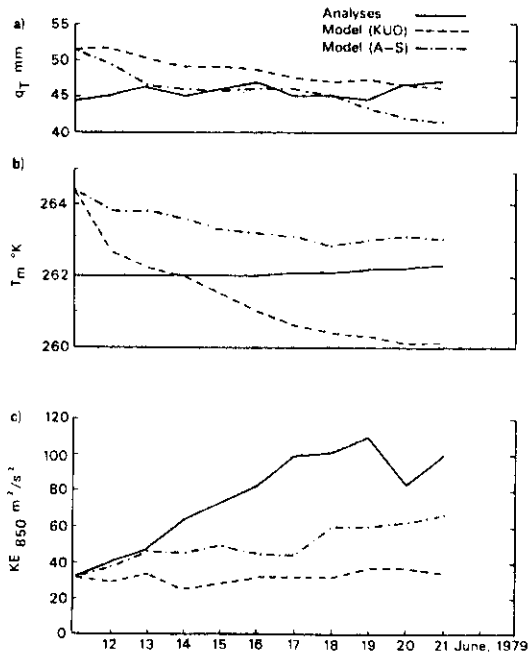

Figure 21. Time sequences of Arabian Sea region averages of (a) total precipitable moisture (mm), (b) tropospheric mean temperature (°K), and (c) kinetic energy per unit mass of 850 mb flow ($m^2 s^{-2}$). Full curves refer to FGGE IIIb analysis, dashed curve Kuo scheme and dash-dot curve A-S scheme

These show both schemes to be deficient in predicting the observed rapid development over the region. The Kuo scheme is particularly bad, also tending to cool the atmosphere by about 2°K over the 10-day period.

Additional insight into the behaviour of the schemes is provided by the distributions of mean tropospheric heating shown in Fig. 22.

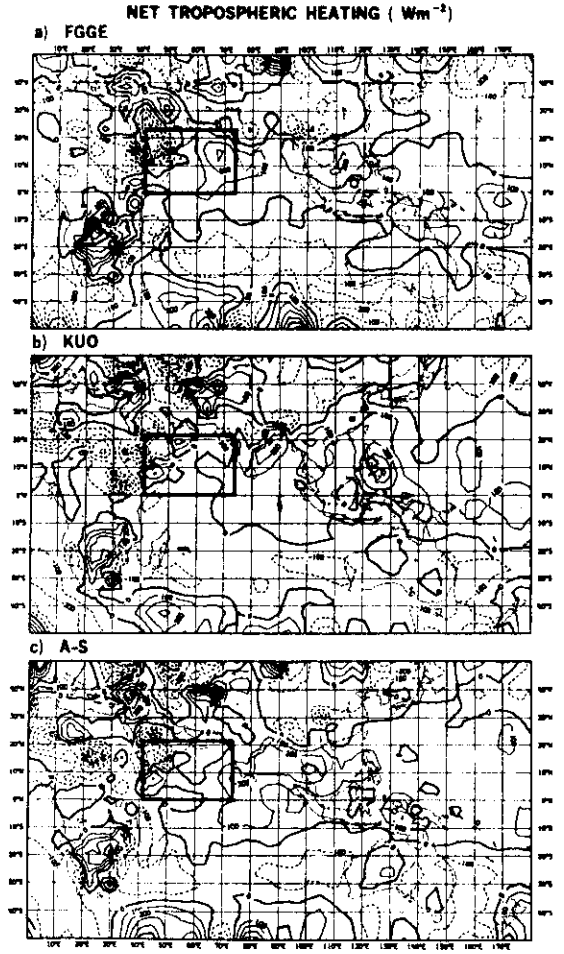

Figure 22. Mean net tropospheric heating (W m^{-2}) from 1200Z on 12 June to 1200Z on 21 June, 1979 (a) from FGGE analyses, (b) from Kuo simulation and (c) from A-S simulation. The Arabian Sea area is outlined.

Essentially the Kuo scheme, although giving some latent heat release over the area (even a zero net heating implies latent heat release of about 100 W m^{-2} - about 4mm of rain per day, since the mean radiative cooling is about 120 W m^{-2}), does not give the observed maximum of about 300 W m^{-2} over the eastern part of the region. The A-S scheme does rather better. Both schemes, however, produce more than the observed rainfall over the Bay of Bengal. One of the reasons for the poor location of the main rainfall region using the Kuo scheme is that it is very sensitive to the divergent part of the low level wind field and so leads to errors if this is in error.

It is interesting that both schemes also predict rain over Libya to the east of the observed rainfall over Algeria.

5.3 General Circulation Model experiments on the climate of the Sahel

These experiments are considered as an example of numerical model experimentation directed towards increased understanding of the physical processes associated with seasonal variability of climate.

Several groups have carried out GCM experiments with global changes in albedo, soil moisture and evaporation over land (see, e.g., review by Mintz (1984) in 'Global Climate', Ed. J.T. Houghton, Cambridge University Press, pp 79-105). The possibility of a positive albedo feed-back leading to drought has been much discussed and is on the whole supported by model experiments; this effect arises from the tendency for drying vegetation to imply an increase in surface albedo. In model integrations there is an initial reduction of absorption of solar radiation by the ground, and of transport of sensible and latent heat to the atmosphere. There is less convective cloud and this allows more solar radiation to reach the ground, compensating for the initial decrease. But it reduces the downward long-wave flux even more so that the net radiative absorption is decreased, implying lower evaporation rate and lower rainfall. Generally, as might be expected, there is a clear decrease in rainfall when evaporation over land is reduced for whatever reason. An exception was an experiment carried out by Sud and Fennessy (Journal of Climatology, pp 383-398) in which they suppressed all evaporation over the Sahel region; rainfall actually increased there because the surface pressure was lower than in the control run and the lack of evaporation was more than offset by moisture import into the region associated with increased low level convergence. Their experiment illustrates the complexity of the situation and the need for carefully designed numerical experiments if a proper understanding is to be achieved of the interactions between evaporation, albedo changes, biomechanisms and atmospheric dynamics.

An an example of a recent such experiment carried out by Rowntree, Wilson and Sangster of the U.K. Meteorological Office, Figures 23(b) and (c) show the differences in seasonal (June-August) rainfall over W. Africa resulting from reduced soil water capacity (from 15 cm to 1 cm) starting from March 1st of Year 2 of a 4½ year control experiment starting in July of year 0 (Fig.23(a)).

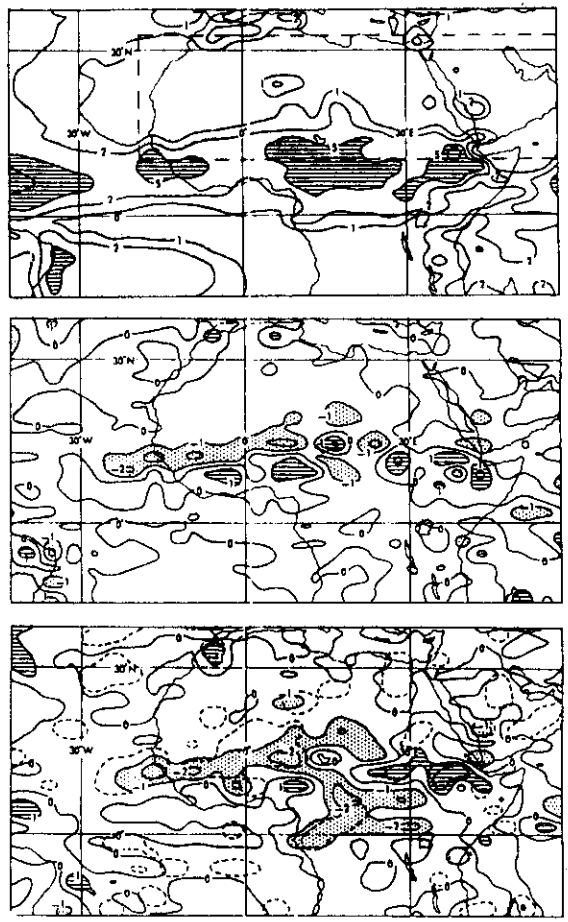

Figure 23. (a) Precipitation (mm/d) averaged for Jun to Aug of Years 1 to 4 of the control experiment which started on 24 July of Year 0. Contours at 1,2,5, 10 mm/d. Areas with over 5 mm/d shaded. The area with reduced moisture capacity is dashed.
(b) and (c): Differences in rainfall (mm/d), relative to the control average for Jun to Aug of experiments with reduced soil water capacity starting from 1 Mar of (b) Year 2 and (c) Year 3 of the control experiment. Contours at 0, 1, 2, 5 mm/d with increases(decreases) of over 1 mm/d hatched(stippled).

The formulation of evaporation (E) was to take $E = \beta E_p$ where the potential evaporation E_p allowed for a typical surface resistance of 60 s m^{-1}; here $\beta = m/m_c$, $m < m_c$, and $\beta = 1$ for $m > m_c$ where m is the soil moisture and $m_c = 5$ cm. Run-off in rivers or to ground water only occurs if $m > m_{max}$ where m_{max} = 15 cm in the control run and 1 cm over the region 10 - 32½ °N, 20W - 60E in the anomaly experiments. Both anomaly experiments show a reduction of over 1mm/day over the region from Senegal to Niger, with fairly systematic increases further east. The latter are associated with increased poleward flow of moist boundary layer air on the eastern side of a low pressure anomaly over the warmer area of reduced soil moisture.

LECTURE 6 PLANETARY SCALE PHENOMENA AFFECTING SEASONAL AND INTERANNUAL VARIABILITY IN THE TROPICS - THE 30-60 DAY OSCILLATION AND EL NINO

It is now generally accepted that interannual variability of regional phenomena such as those discussed in the last lecture depends not only on the seasonal cycle but on additional long period planetary phenomena. The first of these to be identified (by Walker in the 1920's) was the Southern Oscillation (SO). Then, when tropical upper air observations became routinely available, in the 1950's, the quasi-biennial oscillation (QBO) was discovered. El Niño (EN), the occurrence of exceptionally warm water off the coast of Peru, has been recognised for a century or more through its effect on the fishing industry there. Strong linkages between the EN and SO are now well established (see Fig. 4 of 'The Global Climate System') based on detailed observations over the last 50 years and their combination is referred to as ENSO. The 30-50 day oscillation in the tropics was first identified by Madden and Julian (1971, J. Atmos. Sci., pp 702-708).

6.1 The 1982/3 ENSO

This is described in detail in 'The Global Climate System'. Its study is a major component of the WMO/ICSU Tropical Ocean Global Atmosphere (TOGA) project, a component of the World Climate Research Programme (WCRP).

Useful insight into the dynamics of the atmospheric response to tropical heat sources, in particular during ENSO events, has recently been provided by Sardeshmukh and Hoskins (Q.J. Roy. Met. Soc., 1985, pp 261-278). They consider in detail the steady state response of the observed steady zonal mean flow to the observed 150 mb divergence associated with the heating anomaly, adopting for this purpose the barotropic vorticity equation in p-coordinates

$$\frac{\partial \zeta}{\partial t} + \underline{v}\cdot\nabla(\zeta + f) + \underline{k}\cdot\nabla \times \omega \frac{\partial \underline{v}}{\partial p} = - (\zeta + f)\nabla\cdot\underline{v} \quad , \tag{12}$$

where ζ denotes the relative vorticity. They show, using FGGE data for DJF 1982/3, that, taking time averages over a season (denoted by $\bar{}$), this may be approximated as

$$\bar{\underline{v}}\cdot\nabla(\bar{\zeta} + f) = - (\bar{\zeta} + f)\nabla\cdot\bar{\underline{v}} \quad , \tag{13}$$

i.e., the tendency and twisting terms and transients are negligibly small. They then take the further step of linearising the longitudinally varying time-mean flow about the zonal mean $[\bar{u}]$, i.e. approximate (13) as

$$[u]\frac{\partial \bar{\zeta}^*}{\partial x} + v^* \frac{\partial}{\partial y}\left([\bar{\zeta}] + f\right) = - \left([\bar{\zeta}] + f\right)\nabla\cdot\underline{v}^* \quad , \tag{14}$$

where * denotes a deviation from the zonal average. The left-hand side of (14) is a much better approximation to the stretching term on the right than the widely used $\beta\bar{v}$ of the Sverdrup balance, implying that one cannot linearise about a basic state at rest in the tropics (as in Gill's 1980 model) because $\beta - \frac{\partial^2 \bar{u}}{\partial y^2}$ is significantly smaller than β over large areas. The Sverdrup balance is, however, quite reasonable at lower levels where $[\bar{u}]$ is smaller.

Eq. (14) was integrated by introducing a streamfunction ψ^* $\left(v^* = \frac{\partial \psi^*}{\partial x}\right.$, $u^* = - \frac{\partial \psi^*}{\partial y}$, $\bar{\zeta}^* = \nabla^2\psi^*$, specifying $\nabla\cdot\underline{v}^*$ and introducing a frictional damping $- r\nabla^2\psi^*$ on the right-hand side. The resulting ψ^*, with r^{-1} = 2.6 days, is shown in Fig. 24(a); the observed perturbation streamfunction is shown in Fig. 24(b).

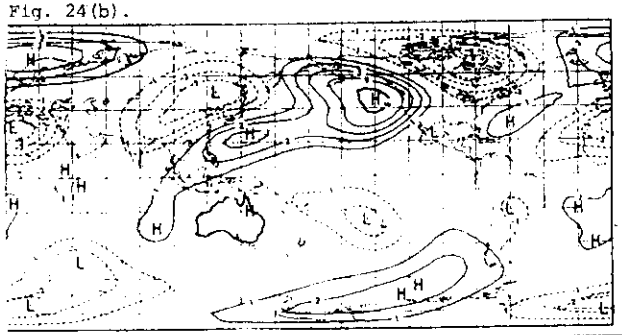

(a)

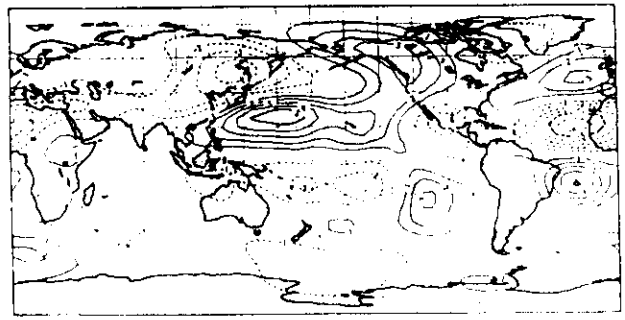

(b)

Figure 24

(see text)

The agreement is most encouraging, strongly supporting the approximations made. It provides a particularly straightforward interpretation of the upper flow response to large-scale heat sources in the tropics, where, because latent heat release in deep convective systems is involved, the upper divergence is located directly over the heat source region - in this case characterised by a high SST. This analysis strongly emphasises the importance of non-linear effects, particularly near the equator.

6.2 The 30-60 day oscillation

Sardeshmukh and Hoskins also drew attention to the existence of a low frequency periodicity of 30-60 days in the 150 mb divergence during DJF 1982/3. Fig. 25 compares this with observations of outgoing longwave radiation during the period.

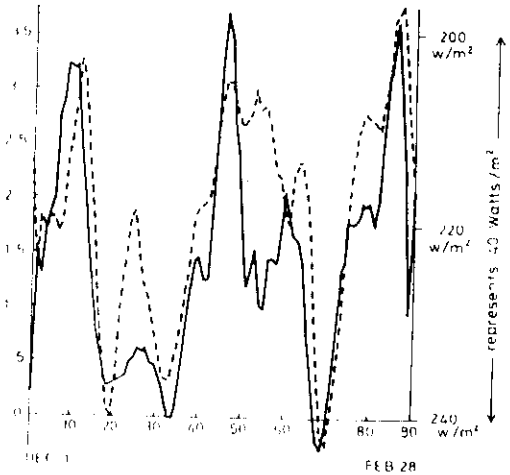

5-day running means of the 150 mb divergence (solid line) and outgoing longwave radiation (dashed line) averaged over the area 5°N-25°S, 165°W-135°W in the central Pacific during D.J.F. 1982/83. Units are 10^{-6} s^{-1} for the divergence and W m^{-2} for o.l.r.

Figure 25

Krishnamurti and Gadgil (1985, Tellus, pp 336-360) have analysed the complete FGGE IIIb data produced by ECMWF and succeeded in generating a time sequence of 850 mb streamline charts giving the global structure of the wave and its evolution for DJF. The 850 mb wind (streamline) patterns for 10 Dec 1978

and 4 Feb 1979 are reproduced below as Figure 26.

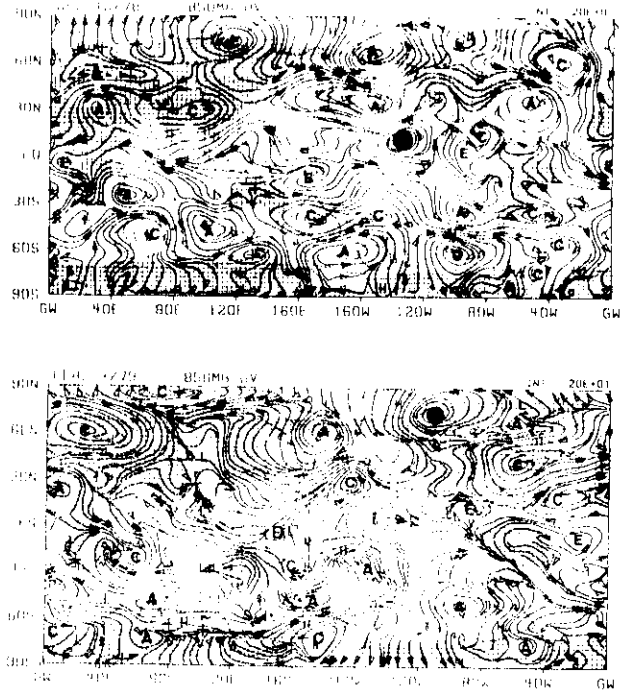

Figure 26

These illustrate the essentially global extent of the phenomenon. It is possible to follow the movement of particular features over the period, e.g. the cyclonic cell denoted by the black dot moves steadily polewards over the 60 day period. The wind just polewards of its initial position (15°N, 130°W) undergoes two reversals of direction during this period. The general tendency is for such patterns to migrate polewards, suggesting that these are disturbances which originate in the tropics and are linked with convective activity there.